ELSEVIER

Journal of Alloys and Compounds 408–412 (2006) 706–710

Journal of ALLOYS AND COMPOUNDS

www.elsevier.com/locate/jallcom

Fluorescence of Ce^{3+} in fluorides and long-lasting phosphorescence of Ce^{3+} in oxides

Mitsuo Yamaga [a,*], Nobuhiro Kodama [b]

[a] *Department of Mathematical and Design Engineering, Gifu University, Gifu 501-1193, Japan*
[b] *Department of Materials Science and Engineering, Akita University, Akita 010-8502, Japan*

Received 2 August 2004; received in revised form 16 December 2004; accepted 13 January 2005
Available online 23 May 2005

Abstract

Fluoride crystals, $LiYF_4$ and $LiCaAlF_6$, doped with Ce^{3+} are useful for ultraviolet tunable lasers because of large band gaps. Although oxide crystals doped with Ce^{3+} are not useful for lasing, they have an advantage to scintillators and new passive optical sources. Such optical properties of Ce^{3+} strongly depend on host crystals.

Keywords: Ce^{3+}; Fluoride crystals; Oxide crystals; Crystal field; Laser materials; Scintillators; Long-lasting phosphorescence

1. Introduction

Ce^{3+}-doped materials are attractive for applications to lasers, scintillators, and phosphors [1]. Laser action in the ultraviolet (UV) range has been performed using $LiYF_4$:Ce^{3+} [2], $LiLuF_4$:Ce^{3+} [3,4] and $LiCaAlF_6$:Ce^{3+} [4] because the fluoride crystals have high energy band gaps. However, it has not been achieved for oxide crystals, for example, $Y_3Al_5O_{12}$ (YAG):Ce^{3+} [5] because of the excited state absorption (ESA). Recently, Lu_2SiO_5 (LSO):Ce^{3+} [6] and $LuAlO_3$:Ce^{3+} [7] were developed as new scintillators having high conversion efficiency from high energy to visible light. In addition, long-lasting phosphorescence in $Ca_2Al_2SiO_7$:Ce^{3+} [8], which is a great disadvantage to the above two applications, has been attractive for new passive optical sources emitting persistently for several hours.

The Ce^{3+} luminescent materials have a variety of applications, which depend on host crystals. In this paper, we discuss optical properties of Ce^{3+}-doped fluoride and oxide single crystals in which the effects of the strength and symmetry of the crystal field depending on host crystals can be assessed. Furthermore, a new model of a mechanism that the afterglow observed in $Ca_2Al_2SiO_7$:Ce^{3+} persists for several hours after removal of excitation is proposed.

2. Crystal field splitting of Ce^{3+} in crystals

The lowest energy state of Ce^{3+} in crystals has a single 4f electron outside the closed shells. The state is split into $^2F_{5/2}$ and $^2F_{7/2}$ with separation energy of 2250 cm^{-1} by spin–orbit interaction. The next highest state with 30,000–60,000 cm^{-1} in energy has a 5d electron. The 4f ↔ 5d transitions corresponding to optical absorption and fluorescence of Ce^{3+} in crystals are parity- and spin-allowed so that lifetimes of the fluorescence are in the range of 10–60 ns.

The spatially diffuse 5d electron orbital extends outward from the ion to overlap the neighbouring ligand ions, and is more strongly influenced by their motion. In consequence, the optical properties depend strongly on structure of host crystals.

Fig. 1 shows schematic energy levels of the 4f and 5d states of Ce^{3+} in cubic crystal field. The 5d excited state is split into E and T_2 orbital states with separation energy of 10Dq. The magnitude of 10Dq is determined by distances between Ce^{3+} and ligand ions, valence of ligand ions, and

* Corresponding author. Tel.: +81 58 293 3052; fax: +81 58 293 3052.
E-mail address: yamaga@cc.gifu-u.ac.jp (M. Yamaga).

0925-8388/$ – see front matter © 2005 Elsevier B.V. All rights reserved.
doi:10.1016/j.jallcom.2005.01.092

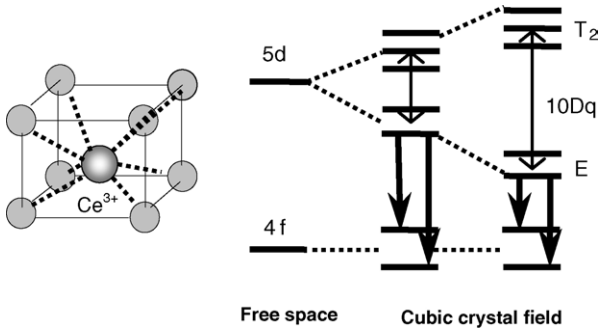

Fig. 1. Schematic energy levels of 4f and 5d states of Ce^{3+} in cubic crystal field.

number of surrounding ligand ions. In a strong crystal field, the five absorption bands spread toward high and low energies so that luminescence is red-shifted.

Fig. 2 shows the typical vacuum ultraviolet (VUV) and UV absorption and UV fluorescence spectra in CaF_2 crystals codoped with Ce^{3+} and Na^+ as charge compensators. Two groups of the broad bands are composed with 303 nm, and 179, 186 and 192 nm. These bands correspond to the transitions from the $^2F_{5/2}$ ground state of the 4f configuration to the ^2E and $^2T_2$ excited states of the 5d configuration of Ce^{3+}, respectively, as shown in Fig. 1. These bands have been assigned as being due to the transitions from cubic centers [9,10]. The UV fluorescence has double peaks at 315 and 335 nm corresponding to the ground state splitting.

When anions are changed from fluorine to oxygen ions, the crystal field is enhanced because the change in the valence of the anions is from −1 to −2. Then, the crystal field of Ce^{3+} in oxide crystals is increased so that the fluorescence is red-shifted as shown in Fig. 1. The peak wavelengths of the Ce^{3+} luminescence bands in $Ca_2Al_2SiO_7$ [8] and YAG [5], being located at 410 and 560 nm, respectively, are shifted toward

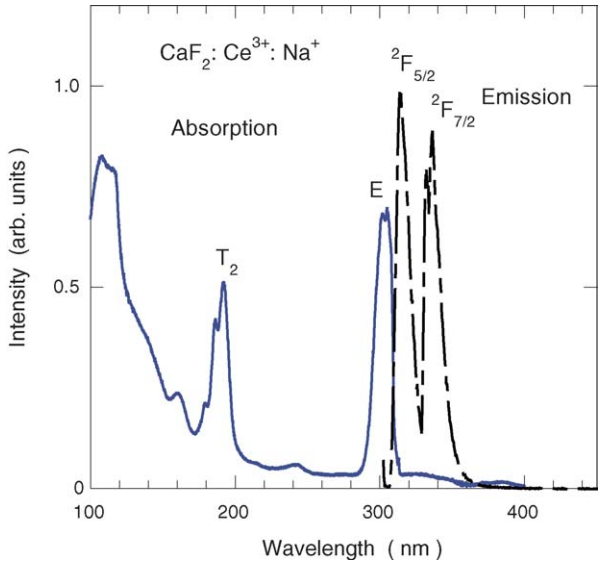

Fig. 2. VUV/UV absorption and UV fluorescence spectra of Ce^{3+} in CaF_2:0.01% Ce^{3+}:1% Na^+ measured at 15 K.

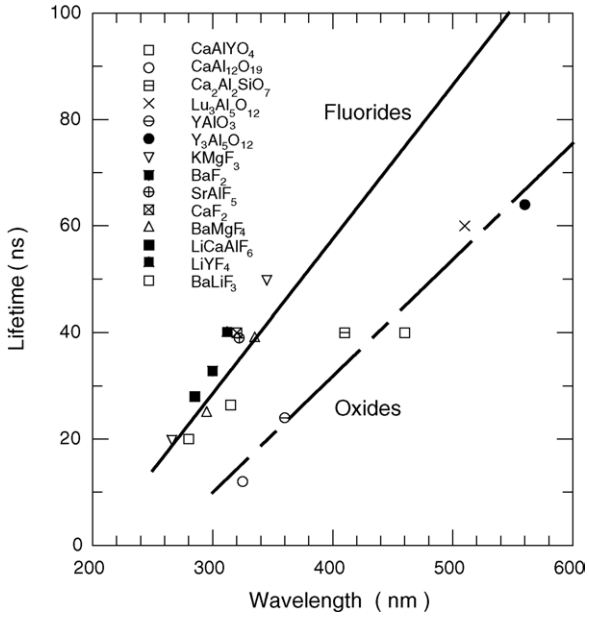

Fig. 3. Relationship between peak wavelengths and lifetimes of Ce^{3+} fluorescence in various fluoride and oxide crystals.

long wavelengths compared with those observed in fluoride crystals. The red-shift of the luminescence is also caused by the nephelauxetic effect [11].

Fig. 3 shows the relationship between the peak wavelengths and lifetimes of the Ce^{3+} luminescence in various fluoride and oxide crystals [12]. The lifetimes (40 ns) of Ce^{3+} in CaF_2, $SrAlF_5$, $LiYF_4$ and $BaMgF_4$, where Ce^{3+} is eightfold-coordinated, are close to each other. The lifetimes in fluorides are distributed in the range of 20–50 ns. The variations of the lifetimes and the wavelengths in the oxides are larger than those in fluorides. The 560 nm luminescence with the lifetime of 60 ns in YAG:Ce^{3+} shows the largest red-shift in Fig. 3. The slope of the lifetime versus wavelength in the oxides is slightly smaller than in the fluorides.

The strength of the crystal field is associated with the size of complexes composed of central Ce^{3+} and anion ligand ions. As the size becomes small, that is, the distances between Ce^{3+} and ligand ions are short, mixing the wavefunctions of Ce^{3+} and ligand ions is enhanced. Then, the center of gravity of the 5d excited state energy levels is reduced. This phenomenon is called as the nephelauxetic effect [11]. Lowering symmetry, which is associated with odd-parity distortion of the complexes, mixes the opposite-party wavefunctions into the wavefunctions of the ground and excited states. For example, the 4f-orbital wavefunction of the ground state mixes with the 2s-orbital wavefunctions of ligand ions of F^- or O^{2-}, while the 5d-orbital wavefunctions of the excited states mixes with the p-orbital wavefunctions of Ce^{3+} and/or ligand ions. The large mixing coefficients are associated with the energy shift of the lowest excited state to lower energy as shown in Fig. 1. The enhancement of the mixing coefficients reduces the transition probabilities, resulting in increasing the lifetimes of the Ce^{3+} fluorescence. In consequence, the lifetime

versus peak wavelength shows the linearly relation when the fluorescence is red-shifted.

3. Applications

3.1. Laser materials

Laser action in the UV range has been performed using $LiYF_4:Ce^{3+}$ [2], $LiLuF_4:Ce^{3+}$ [3,4] and $LiCaAlF_6:Ce^{3+}$ [4]. Substitution of Ce^{3+} for Y^{3+} in $LiYF_4$ does not require charge compensators because of the same valence of Ce^{3+} and Y^{3+}. On the other hand, Ce^{3+} ions substitute for Ca^{2+} in $LiCaAlF_6$ accompanied by charge compensators. The charge balance between Ce^{3+} and Ca^{2+} is compensated by replacement of Ca^{2+} with Li^+ or dopant Na^+. An excess of the charge compensators leads to reduction of optical quality of crystals, that is, creation of cation and anion vacancies in crystals. In the case of $LiCaAlF_6:Ce^{3+}$, pump-induced solarization prevented laser operation [13]. However, the improvement of the optical quality could achieve laser operation in $LiCaAlF_6$ doped with a single Ce^{3+} ion and codoped with Ce^{3+} and Na^+ ions [4].

Recently, laser materials operating at near 200 nm is required. In order to satisfy this requirement, laser materials are designed taking account of the crystal field of Ce^{3+} surrounding in host crystals and crystal growth with high optical quality without vacancies. Materials design is as follows: (1) choice of fluorides as shown in Fig. 3; (2) a decrease of number of ligand ions, for example, from cube to octahedron; (3) larger distances between Ce^{3+} and ligand ions; (4) high symmetry (cubic symmetry). Fluoride crystals with perovskite structure are candidates for laser host crystals.

Another method is frequency doubling using non-linear materials. There are a few of fluoride crystals having a non-linear effect. $BaMgF_4$ (BMF) crystals [14] are a candidate for laser host crystals with a non-linear effect. Optical and crystalline properties of the $BMF:Ce^{3+}:Na^+$ crystal have been reported by Yamaga et al. [15]. Two luminescence spectra with different peak wavelengths observed in BMF are assigned to two Ce^{3+} centers: one is a Ce^{3+} center occupied at perfect lattices reflecting superlattice structure; the other is a Ce^{3+} center perturbed by charge compensators Na^+. Strong UV excitation produces coloration of the crystal corresponding to electron and hole trapping, resulting in no lasing [16]. Whether the $BMF:Ce^{3+}:Na^+$ crystal performs lasing or not strongly depends on the optical quality of the host crystals. Excesses of Na^+ produce F^- vacancies in the crystal, resulting in reduce the optical quality. In order to obtain the high quality crystal with less F^- vacancies keeping charge balance between Ce^{3+} and Na^+, the most suitable growth conditions should be found through changing the melting temperature, the pressure of the growth atmosphere, and the ratio of starting compounds of BaF_2, MgF_2, CeF_3 and NaF. If the crystals with less F^- vacancies are obtained through the above best growth conditions, it is possible to operate lasing in the wavelength of 150–200 nm.

3.2. Long-lasting phosphors

UV excitation in the Ce^{3+} absorption bands of $Ca_2Al_2SiO_7:Ce^{3+}$ at room temperature produces an intense broadband of the Ce^{3+} fluorescence with a peak wavelength of 410 nm and a lifetime of 40 ns and simultaneously phosphorescence with the same line shape of the fluorescence and fairly wide decay times of $1–10^3$ s [8]. Laser action could not be achieved using $Ca_2Al_2SiO_7:Ce^{3+}$.

Fig. 4 shows the decay curves of the phosphorescence for $Ca_2Al_2SiO_7:Ce^{3+}$ in the time range of $5–10^3$ s in log–log scales. The decay curve at 306 K fits a function of $t^{-0.56}$. At 400 K, the initial intensity is about one order of magnitude larger than that at 306 K. The decay curve at 500 K fits a function of $t^{-0.86}$.

Before we consider a mechanism of the long-lasting phosphorescence, it is very important to understand how UV excitation energy is stored in the crystal at low temperatures. In the previous paper [8], we have reported the ESR results that electrons and holes produced in $Ca_2Al_2SiO_7:Ce^{3+}$ by UV excitation at low temperatures are trapped at oxygen vacancies in the form of F^+ center and self-trapped at AlO_4 tetrahedra, respectively.

Let us consider the properties of the long-lasting phosphorescence, taking account of the above ESR results. As the line shape of the phosphorescence is coincident with that of the fluorescence, self-trapped holes (STH) should move in the crystal and again be captured at Ce^{3+}. It is assumed that an STH hops to an adjacent AlO_4 tetrahedron through thermal activation energy as shown in Fig. 5 and the hopping rate is enhanced in increasing temperature. This assumption can

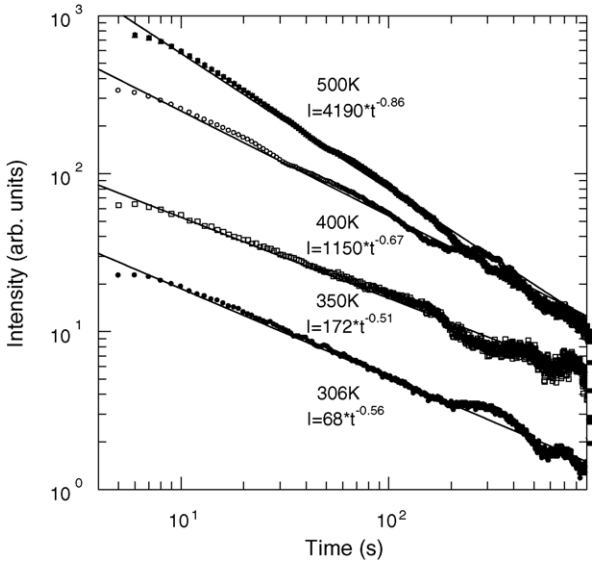

Fig. 4. Decay curves of phosphorescence for $Ca_2Al_2SiO_7:Ce^{3+}$ at various temperatures.

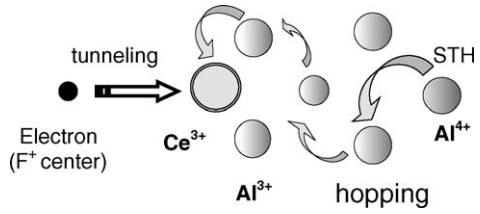

Fig. 5. Schematic diagram of hopping process of self-trapped holes in the form of AlO_4 in $Ca_2Al_2SiO_7$ and electron–hole recombination process at Ce^{3+} site.

explain enhancement of the phosphorescence in increasing temperature 306–400 K.

Here, we discuss the hopping process using the decay curves of the phosphorescence in Fig. 4. The decay curve at 500 K fits a function of $t^{-0.9}$. As the decay curve of radiative recombination of electrons and holes caused by tunneling can be represented by t^{-1} [17], it is expected that holes (Ce^{4+}) localized at Ce^{3+} recombine radiatively with nearby trapped electrons by tunneling as shown in Fig. 5. On the other hand, the decay curves at 306 and 350 K fit a function of $t^{-0.5}$, that is, the phosphorescence at 306 and 350 K persist for longer times than that at 500 K. Therefore, this difference deduces information on the thermal hopping of STH.

A succession of phonon-assisted hopping of STH is strongly associated with a diffusion process. The diffusion constant is given by $D = a^2R$, where a is the distance between two adjacent STHs and R is the hopping rate of STH. A diffusion time t_d of STH to Ce^{3+} sites is given by $t_d = r^2/D$, where r is the distance between STH and Ce^{3+}. STHs produced by UV excitation at low temperatures are distributed in the crystals. Taking account of the diffusion process, the number of holes captured at Ce^{3+} sites at $t = t_d$ is proportional to the distribution function, $n(r)$, of STH in the crystal. The decay curve of the long-lasting phosphorescence produced by two processes of hopping motion of STH and tunneling recombination is represented by convolution of $n(r)$ and t^{-1} satisfying the relation of $r = \sqrt{tD}$. The observed decay curve with a function of $t^{-0.5}$ fits the convolution function calculated with an assumption that a distribution function of $n(r)$ is independent of r. In consequence, the different decay curves at 306–500 K deduce hopping motion of STH around room temperature.

4. Conclusions

The fluoride crystals, $LiYF_4$ and $LiCaAlF_6$, doped with Ce^{3+} are useful for UV tunable lasers because of the wide band gaps. However, UV tunable laser materials have not been found in other fluoride. Whether crystals perform lasing or not strongly depends on optical quality of host crystals other than the wide band gap. If Ce^{3+}-doped $BaMgF_4$ and other fluoride crystals with perovskite structure with less F^- vacancies are obtained through the improved growth conditions, it is possible to operate lasing in the wavelength of 150–350 nm.

Although oxide crystals doped with Ce^{3+} are not useful for lasing, they have an advantage to scintillators and new passive optical sources. X-ray irradiation produces electron–hole pairs in crystals. If electron–hole pairs recombine radiatively at Ce^{3+} sites, intense Ce^{3+} fluorescence can be observed with short lifetimes in the range of 20–60 ns. However, holes created by X-ray or UV excitation in some oxides are self-trapped at cation lattice sites, for example, Al^{3+} site forming AlO_4 tetrahedra in $Ca_2Al_2SiO_7$ [8]. If self-trapped holes are stable at room temperature, the electron–hole recombination creates background emission, that is, afterglow. Scintillator materials are required to reduce this background emission. On the other hand, a new passive optical source takes an advantage of the afterglow persistently for several hours. Therefore, we must design separately host crystals doped with Ce^{3+} ion for applications to scintillators or passive optical sources because such optical properties of Ce^{3+} strongly depend on host crystals.

Acknowledgments

This work was in part supported by a Grant-in-Aid for Science Research (C) from Japan Society for the Promotion of Science (No. 14550037). One of the authors (M. Yamaga) is indebted to the Iwatani Naoji Foundation for a Research Grant.

References

[1] G. Blasse, B.C. Grabmaier, Luminescent Materials, Springer, Berlin, 1994.
[2] T.D.J. Ehrlich, P.F. Moulton, R.M. Osgood, Opt. Lett. 4 (1978) 184.
[3] I.M. Raieri, K. Shimamura, K. Nakano, T. Fujita, Z. Liu, N. Sarukura, T. Fukuda, J. Cryst. Growth 217 (2000) 151.
[4] N. Sarukura, M.A. Dubinskii, Z. Liu, V.V. Semashko, A.N. Naumov, S.L. Korableva, R.Y. Abdulsabirov, K. Edamatsu, Y. Suzuki, T. Itoh, Y. Segawa, IEEE J. Sel. Top. Quantum Electron. 1 (1995) 792.
[5] D.S. Hamilton, S.K. Gayen, G.J. Pogatshnik, R.D. Ghen, W.J. Miniscalco, Phys. Rev. B 39 (1989) 8807.
[6] L.A. Kappers, R.H. Bartram, D.S. Hamilton, A. Lempicki, J. Glodo, J. Lumin. 102–103 (2003) 162.
[7] A.J. Wojtowicz, P. Szupryczyhski, D. Wisniewski, J. Glodo, W. Drozdiwski, J. Phys.: Condens. Matter 13 (2001) 95.
[8] M. Yamaga, Y. Tanii, N. Kodama, T. Takahashi, M. Honnda, Phys. Rev. B 65 (2002) 235108.
[9] D.W. Pack, W.J. Manthey, D.S. McClure, Phys. Rev. B 40 (1989) 9930.
[10] L. van Pieterson, M.F. Reid, R.T. Wegh, S. Soverna, A. Meijerink, Phys. Rev. B 65 (2002) 045113.
[11] B. Henderson, G.F. Imbusch, Optical Spectroscopy of Inorganic Solids, Clarendon Press, Oxford, 1989, p. 390.
[12] M. Yamaga, T. Imai, H. Miyairi, N. Kodama, J. Phys.: Condens. Matter 13 (2001) 9753.
[13] C.D. Marshall, J.A. Spaeth, S.A. Payne, W.F. Krupke, G.J. Quarles, V. Castillo, B.H.T. Chai, J. Opt. Soc. Am. B 11 (1994) 2054.

[14] S.C. Buchter, T.Y. Fan, V. Liberman, J.J. Zayhowski, M. Rothschild, E.J. Mason, A. Cassanho, H.P. Jenssen, J.H. Burnett, Opt. Lett. 26 (2001) 1693.
[15] M. Yamaga, K. Hattori, N. Kodama, N. Ishizawa, M. Honda, K. Shimamura, T. Fukuda, J. Phys.: Condens. Matter 13 (2001) 10811.
[16] E. Hayashi, S. Yabashi, M. Yamaga, N. Kodama, S. Ono, N. Sarukura, J. Alloys Compd. 408–412 (2006) 883–885.
[17] S.W.S. Mckeever, Thermoluminescence of Solids, Cambridge University Press, Cambridge, 1985, p. 143.